PAPER

Check for updates

Cu/ZnOx@UiO-66 synthesized from a double solvent method as an efficient catalyst for CO2 hydrogenation to methanol†

Yang Yang,‡[a] Yanan Xu,‡[a] Heng Ding,[a] Dong Yang,[a] Enping Cheng,[a] Yiming Hao,[a] Hongtao Wang,[a] Yanzhen Hong,[a] Yuzhong Su,[a] Yanliang Wang,*[a] Li Peng*[a] and Jun Li [iD] *[abc]

Cu/ZnOx in UiO-66, namely, Cu/ZnOx@UiO-66, was synthesized using a double solvent method with controllable Cu/Zn ratios. Due to the ultra-small nanoparticles confined in the metal–organic framework and the special Cu/ZnOx interface, this composite Cu/ZnOx@UiO-66 catalyst showed excellent performance for CO2 hydrogenation to methanol. In fact, the space–time yield of methanol is enhanced by 5.5 and 8.5 times compared with those on the commercialized Cu/ZnO/Al2O3 and the Cu/ZnOx@UiO-66 prepared with the traditional impregnation method. Furthermore, the catalyst shows good stability over a period of 100 h on stream.

1. Introduction

Although the excessive emission of CO_2 has brought many environmental problems, CO_2, as an abundant, cheap, non-toxic and easily achievable C1 feedstock, can be converted into value-added chemicals through various chemical methods, which has attracted extensive attention.[1–3] Among all the alternatives, catalytic hydrogenation of CO_2 to methanol is one of the most promising approaches.[4–6] Methanol is widely recognized as a clean fuel that can be used directly and it can also be converted to valuable products such as olefins, formaldehyde, methyl methacrylate, acetic acid and methylamines.[7–9] The ternary $Cu/ZnO/Al_2O_3$ catalyst is usually used for producing methanol industrially from syngas (CO/CO_2/H_2) or from CO_2 hydrogenation.[10,11] Unfortunately, this catalyst often suffers from the aggregation of Cu nanoparticles (NPs) and the phase separation of Cu and ZnO during the high temperature reaction.[12] Since the Cu/ZnO interface plays a vital role in the activity, phase separation would reduce these important sites, and the aggregated Cu NPs contribute to the reverse water–gas reaction (RWGR), resulting in

reduced selectivity.[13,14] Thus it is important and necessary to find a solution for stabilizing mixed Cu/ZnO interfaces to maintain high catalytic activity and selectivity.

Metal–organic frameworks (MOFs),[15] constructed from metal ions or clusters interlinked with organic ligands, have shown great potential for catalyst preparation due to their unprecedented accessible surface areas, adjustable pore size, good thermal stability and surface functionality.[16–19] MOFs could serve as good supports to stabilize nanoparticles for the preparation of MOF/nanoparticle catalysts.[20,21] Cu⊂UiO-66 synthesized by encapsulating 18 nm Cu NPs into UiO-66 has been reported for its high selectivity for CO_2 hydrogenation to methanol.[22] UiO-67 and its isostructural MOFs, for example, UiO-bpy, are also excellent supports for the preparation of catalysts.[23] The Cu/ZnOx@UiO-bpy catalyst shows high activity, which is attributed to the ultrasmall Cu/ZnOx nanoparticles anchored by the secondary building units (SBUs). The Cu/ZnO@UiO-66 catalyst could also be prepared by the metal organic chemical vapour deposition (MOCVD) method described by Müller *et al.* The size of Cu nanoparticles is around 10–20 nm and the volatile precursor $CpCu(PMe_3)$ must be needed which is quite expensive.[24] Preparing small nanoparticles confined in MOFs without organic coordinating groups is still challenging, for which normally an impregnation method is employed.

The traditional impregnation method is a convenient and effective way to load the metals into MOFs.[25,26] However, when we tried to load Cu and Zn species into MOFs, it was found that the metals easily aggregated into larger nanoparticles on the surface of the MOF crystal (Fig. 1a), which led to phase separation of Cu and Zn at a larger scale. In our

[a] *College of Chemistry and Chemical Engineering, Xiamen University, Xiamen 361005, China. E-mail: ylwang@xmu.edu.cn, li.peng@xmu.edu.cn, junnyxm@xmu.edu.cn*

[b] *National Engineering Laboratory for Green Chemical Productions of Alcohols, Ethers and Esters, Xiamen University, Xiamen 361005, China*

[c] *Collaborative Innovation Center of Chemistry for Energy Materials, Xiamen 361005, China*

† Electronic supplementary information (ESI) available: Characterization. See DOI: 10.1039/d0cy02450c
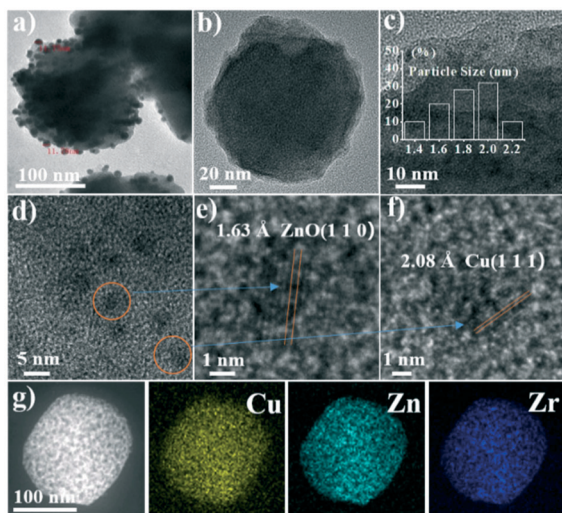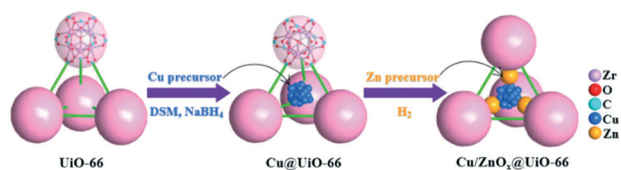
‡ These authors contributed equally.

This journal is © The Royal Society of Chemistry 2021

Catal. Sci. Technol., 2021, **11**, 4367–4375 | **4367**

Fig. 1 (a) TEM image of Cu/ZnO on UiO-66 synthesized by the traditional impregnation method. (b–f) TEM and HRTEM images of Cu/ZnOₓ@UiO-66 synthesized by the double solvent method. (g) HAADF-STEM image and STEM-EDXS elemental maps for Cu, Zn and Zr of Cu/ZnOₓ@UiO-66.

previous work with a MOF/polymer composite, a double solvent method was used to load the polymer precursor into MOF pores and the MOF/polymer composite formed with almost all the polymer inside the pores *via in situ* polymerization.[16] Inspired by this impressive work, we demonstrate that the double solvent method can also effectively introduce Cu into the MOF and make use of the confinement effect of the MOF to prepare smaller nanoparticles. The resulting composite shows a significantly enhanced catalytic activity compared with the commercialized catalyst and the catalyst prepared without the double solvent method.

UiO-66 was chosen as the catalyst support because it is cheap and easy to scale up and it shows good thermal stability.[27–29] This material features $Zr(\mu_3\text{-O})_4(\mu_3\text{-OH})_4$ clusters interlinked by terephthalic acid (bdc) ligands. Since the inner surface of UiO-66 is hydrophilic, it is possible for the Cu precursor to be encapsulated into the hydrophilic pores with the double solvent method. As shown in Scheme 1, dry UiO-66 was firstly soaked in anhydrous hexane, followed by adding a small amount of aqueous solution containing the Cu precursor. By taking advantage of the double solvent method, the aqueous solution tended to diffuse into the pore channel, resulting in an increased amount of Cu precursor that dif-

fused inside the pores. After the reduction of the Cu precursor by NaBH₄ solution, Cu nanoparticles formed within the pores of UiO-66. Zn^{2+} was subsequently introduced into the system by reacting $ZnEt_2$ with the $(\mu_3\text{-OH})$ sites on the MOF structure to obtain the target $Zr_3(\mu_3\text{-OZnEt})$. As is shown in the infrared spectra (IR), the disappearance of the $\nu(\mu_3\text{-OH})$ vibrational band at 3662 cm⁻¹ suggests the occurrence of coordination (Fig. S1†).[30] Cu/ZnOₓ@UiO-66 was then obtained by reducing the catalyst in a fixed bed reactor with reaction gas ($P_{H_2}/P_{CO_2} = 3$; H₂ acted as the reductant).

2. Experimental

2.1 Materials

1,4-Benzenedicarboxylate (99%), zirconium tetrachloride (99%), glacial acetic acid (99.5%), ethanol solution (99.7%), *n*-hexane (97%), dichloromethane (99.5%), *N,N*-dimethylformamide (99.5%), sodium borohydride (98+%), diethylzinc (1.0 M in hexane), copper(ɪɪ) nitrate trihydrate (99%), deionized water and tetrahydrofuran (99.8%) were provided by Sinopharm Group. The synthesis gas (H₂/CO₂/Ar = 72/24/4) was provided by Deli Messel Gas Co., Ltd. Nitrogen (99.9%) was provided by Singapore Aerospace Industries Gas Co., Ltd.

2.2 Synthesis of catalysts

2.2.1 Synthesis of the MOF (UiO-66). UiO-66 was synthesized according to a literature procedure with some modifications. $ZrCl_4$ (100 mg, 0.429 mmol), 1,4-benzenedicarboxylate (bdc, 71 mg, 0.428 mmol), DMF (20 mL), and CH₃COOH (771 mg, 12.861 mmol) were transferred into a volumetric vial and heated at 120 °C for 25 h. After the solution was cooled to room temperature in air, the resulting suspension was collected by centrifugation, washed with DMF several times and dried at 65 °C under vacuum overnight to obtain white powdery UiO-66 (unactivated). After the procedure of solvent replacement with ethanol and drying, the activated UiO-66 was prepared for further use.

2.2.2 Preparation of Cu^{2+}@UiO-66. UiO-66 (1.0 g) was dispersed in 50 mL of anhydrous *n*-hexane and the obtained system was sonicated for 15 min. Then 0.54 mL of aqueous solution of Cu (NO₃)₂·3H₂O (0.2–0.6 g mL⁻¹) was added dropwise under vigorous stirring. After 8 h of stirring, the blue solid adhered to the bottom of the flask. The supernatant was decanted, and the *n*-hexane was distilled off under reduced pressure at 40 °C. The blue sample was then further dried under vacuum at 80 °C overnight to obtain Cu^{2+}@UiO-66.

2.2.3 Preparation of Cu@UiO-66. The obtained Cu^{2+}@UiO-66 was dispersed in 50 mL of CH₂Cl₂ and the mixture was stirred vigorously for 30 min, and 0.47 g NaBH₄ was dissolved in 25 mL of C₂H₅OH for the following reduction process at the same time. The NaBH₄ ethanol solution was then added dropwise into the mixture under an N₂ atmosphere until the colour of the solid turned black totally. The product was dried under vacuum after being centrifuged out and washed with ethanol several times. Then, Cu@UiO-66 was prepared.

Scheme 1 Schematic illustration for the preparation of Cu/ZnOₓ@UiO-66 (DSM: double solvent method).

2.2.4 Synthesis of Cu@UiO-66-(μ_3-OZnEt). Cu@UiO-66 was dispersed in a flask with 50 mL of THF. 2.4 mL of $ZnEt_2$ (1 M in hexane) was added to the flask under an N_2 atmosphere, and then the mixture was stirred overnight. After reaction, the product was centrifuged out and washed with THF more than 3 times. To obtain Cu@UiO-66-(μ_3-OZnEt), the washed product needed to be dried under vacuum overnight.

2.2.5 Synthesis of Cu/ZnO$_x$@UiO-66. Cu@UiO-66-(μ_3-OZnEt) was placed in a fixed-bed reactor and treated with a continuous N_2 flow at a temperature of 250 °C and a pressure of 0.1 MPa for 2 h to remove the air in the reactor and the physical adsorption molecules that may be present on the catalyst. Then, the N_2 flow was replaced with reaction gas (P_{H_2}/P_{CO_2} = 3) under the same conditions for 1 h to reduce Cu@UiO-66-(μ_3-OZnEt) to obtain Cu/ZnO$_x$@UiO-66 *in situ* (H_2 in the reaction gas acted as the reductant).

2.2.6 Synthesis of Cu/ZnO on UiO-66. 0.35 g $Cu(NO_3)_2$, 0.66 g $Zn(NO_3)_2$ and 1.0 g UiO-66 were dispersed in a beaker containing 20 ml ethanol. After ultrasonic dispersion, the mixture was stirred for 3 h to make the MOF in full contact with metal ions. The product was centrifuged out and washed with ethanol at least three times, when the impregnation step was completed. Then Cu^{2+}/Zn^{2+} on UiO-66 was obtained.

Cu^{2+}/Zn^{2+} on UiO-66 was then dispersed in 50 mL of CH_2Cl_2 and, at the same time, 1.0 g $NaBH_4$ was dissolved in 40 mL ethanol to form the solution for the following reduction process. The solution was added dropwise into the system under an inert atmosphere with vigorous stirring. Finally, the sediment was centrifuged out and washed with ethanol several times and Cu/ZnO on UiO-66 was prepared after the process of drying under vacuum.

2.2.7 Synthesis of commercial Cu/ZnO/Al$_2$O$_3$. The synthesis was performed by a co-precipitation method according to a reported procedure with some modifications. 30 mL of 1 M aqueous solution of $Cu(NO_3)_2$, $Zn(NO_3)_2$ and $Al(NO_3)_3$ (6:3:1 atomic ratio) were added dropwise (2 mL min⁻¹) using a syringe pump to 50 mL of deionized water (pH kept at 7 with Na_2CO_3) at 65 °C. Simultaneously, 1.5 M Na_2CO_3 solution was added dropwise in order to keep the pH at 7 ± 0.1. The obtained sediment was aged for 2 h at 65 °C in the mother liquor under vigorous stirring. The sediment was filtered, washed with water, dried at 70 °C and calcined at 350 °C in a muffle furnace.

2.3 Characterization

^{1}H NMR analysis was conducted on a Bruker AVANCE III spectrometer at 400 MHz and the sample digested with HF was dissolved in DMSO-d$_6$. Thermogravimetric analysis (TGA) was performed in air using an SDT-Q600 equipped with an alumina pan. Inductively coupled plasma-optical emission spectrometry (ICP-OES) was performed on an Agilent 720ES. The sample was degraded with aqua regia under ultrasonic treatment. After the product was diluted to a concentration of 10–20 ppm, the experiment was conducted against the traditional six-point method. Powder X-ray diffraction (PXRD)

was carried out on a Rigaku Ultimate IV equipped with graphite monochromatized Cu Kα radiation (λ = 1.54 Å). Nitrogen sorption measurements were conducted with a Micromeritics ASAP 2020 system at 77 K. The samples were pretreated at 120 °C under vacuum for 5 h. The surface area was calculated by the Brunauer–Emmett–Teller (BET) method in the range of P/P_0 = 0.05–0.3. Transmission electron microscopy (TEM) and EDX mapping were performed on a JEOL 1400 and a Phillips Analytical FEI Tecnai (F30) electron microscope. Scanning electron microscopy (SEM) studies were performed on a ZEISS SIGMA.

H_2-Temperature-programmed reduction (H_2-TPR) measurements were conducted by using an Altamira AMI200-R-HP unit with a thermal conductivity detector (TCD) in a 5% H_2–Ar stream (60 mL min⁻¹). The catalyst used for the test should be pretreated for 30 min at a temperature of 250 °C in a N_2 environment to remove the air in the reactor and the physical adsorption molecules that may be present on the catalyst. After the system was cooled to room temperature, the H_2-TPR experiment proceeded with the temperature increased from the room temperature to 250 °C at a heating rate of 5 °C min⁻¹ under a 5% H_2–Ar flow (60 mL min⁻¹).

H_2-Temperature-programmed desorption (H_2-TPD) measurements were conducted by using a Micromeritics AutoChem II 2920 instrument. Before the experiment, the prepared samples should be reduced at 250 °C in a 5% H_2–Ar stream (60 mL min⁻¹) for more than 1 h. After the samples were cooled to room temperature, the purged H_2–Ar stream was switched to a He stream for removing the residual H_2. The H_2-TPD experiment was then conducted when the temperature was increased to 250 °C at a heating rate of 5 °C min⁻¹ and it was held at 250 °C for 1 h. H_2 was monitored by mass spectroscopy (MS, m/z = 2) to avoid the interference of water vapor and CO_2 cracking.

CO_2-Temperature-programmed desorption (CO_2-TPD) measurements were conducted with a Micromeritics AutoChem II 2920 instrument. They have the same pretreated conditions as H_2-TPD. After the possible existing physisorbed molecules on the catalyst were removed by purging a He stream for 30 min, the CO_2-TPD experiment was then operated at 50–250 °C with a heating rate of 5 °C min⁻¹ and the temperature was held at 250 °C for 1 h. CO_2 was monitored by MS.

The DRIFT (diffuse reflectance infrared Fourier transform) spectrum was obtained on a NicoletiS10 *in situ* diffuse reflectance infrared Fourier transform spectrometer. The powder sample was placed in the chamber and reduced by a 5% H_2–Ar mixture (15 mL min⁻¹) at 250 °C with a heating rate of 10 °C min⁻¹. Then, the sample was cooled to room temperature and the physisorbed H_2 was removed by purging He for 30 min for the next test. After the process of reduction, the H_2–Ar stream was replaced with the reaction gas (H_2:CO_2:Ar = 72:24:4, 15 mL min⁻¹) and the temperature was raised at a heating rate of 10 °C min⁻¹. The experiment was then started when the temperature reached 250 °C.

X-ray photoelectron spectroscopy (XPS) measurements were carried out with a Qtac-100 LEISS-XPS spectrometer with

a hemispherical electron energy analyser and a home-made reaction chamber. A monochromatic Al Kα X-ray source (1486.6 eV, anode operating at 300 W) was used as the excitation source. The energy analysis error of the measurement was ±0.2 eV for both binding energy and Auger energy.

2.4 Cu dispersion measurements

The dispersion of Cu was tested on the same instrument (Micromeritics AutoChem 2920 instrument) as the one used to do the H_2-TPD experiment. The sample (100 mg) was pretreated in a 5% H_2–Ar mixture for 1 h at 250 °C to reduce the Cu NPs, and then the sample was cooled to 50 °C and purged with He to remove the residual H_2. Before the final test, the reduced sample needed to be poisoned with N_2O (30 mL min^{-1}) for at least 1 h and then purged with He to remove N_2O. Finally, when the temperature rose to 250 °C and remained steady, the surface Cu^+ ions were reduced in a pulse of 5% H_2–Ar, and the corresponding consumption of H_2 was observed using the thermal conductivity detector. The number of active Cu surface sites was determined using a stoichiometry of 1 Cu_2O:1 H_2:2 Cu for calculation:

$$2Cu + N_2O \rightarrow Cu_2O + N_2$$

$$Cu_2O + H_2 \rightarrow 2Cu + H_2O$$
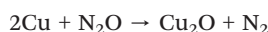
The dispersion of Cu (D_{Cu}) in the catalyst, defined as the number of copper atoms on the surface divided by the total number of copper atoms in the catalyst, was calculated by the equation:

$$D_{Cu} = \frac{2 \times A \times M_{Cu}}{m \times \omega_{Cu}(wt\%)} \times 100\%$$

A is the area of the peak coming from the signals of the TCD, which represents the consumption of H_2. M is the molar mass of Cu (63.546 g mol^{-1}). m is the mass of the catalyst (g) and ω_{Cu} is the mass fraction of Cu.

The turnover frequency (TOF) of product formation was calculated according to the following equation:

$$\text{Turnover frequency (TOF)} = \frac{V_{Formation}}{N_{Cu(surface)}}$$

V represents the formation rate of methanol and N represents the number of Cu surface atoms.

2.5 Catalyst evaluation method

All catalytic tests were performed in a high-pressure continuous-flow fixed-bed reactor. The reaction tube is shown in Fig. S8.† The catalyst was crushed into sheets and then screened to obtain (0.3–0.6 g) particles ranging from 40 mesh to 60 mesh for the tests. Before testing, the catalyst should be pretreated under an N_2 atmosphere (30 mL min^{-1}) with the increase of temperature (2 °C min^{-1}) to remove the air in

the reactor and the physical adsorption molecules that may be presented on the catalyst. After the catalyst was pretreated at the targeted temperature (250 °C) for 1 h, the N_2 flow was switched to H_2 or reaction gas (30 mL min^{-1}) for the reduction reaction. The reduction process usually lasts 3 hours after reaching the set temperature (250 °C).

The catalytic hydrogenation of CO_2 was conducted at a pressure of 4.0 MPa ($H_2/CO_2/Ar = 72:24:4$), a temperature of 180–260 °C and GHSV = 1500–18 000 h^{-1}. Argon was used as an internal standard to reduce systematic error and calculate the conversion rate of CO_2. The products were quantified by gas chromatography with a thermal conductivity detector (TCD) and a flame ionization detector (FID). The columns were TDX-01 for Ar, CO, and CO_2, and Porapak-Q for methanol. The several main indices of the catalyst are calculated as follows, including the conversion rate of reactants (X_{CO_2}), the selectivity to products (S_{CH_3OH}) and the space–time yield (STY).

$$f = \frac{C}{A}$$

C is the concentration, A represents the chromatographic peak areas of different chemicals with a specific mole number and then f is the correction factor defined as C/A for further calculation.

$$X_{CO_2} = \left(1 - \frac{\frac{A_{CO_2}^{out}}{A_{Ar}^{out}}}{\frac{A_{CO_2}^{in}}{A_{Ar}^{in}}}\right) \times 100\%$$

$A_{CO_2}^{in}$ and A_{Ar}^{in} represent the peak areas of the reactants and internal standard gas before the reaction detected using the gas chromatographic TCD.

$$S_{CO} = \frac{A_{CO}^{out} \times f_{CO}}{\left(A_{CO_2}^{in} - A_{CO_2}^{out}\right) \times f_{CO_2}}$$

$$S_{CH_3OH} = \frac{A_{CH_3OH} \times f_{CH_3OH}}{A_{CH_4} \times f_{CH_4} + A_{CH_3OH} \times f_{CH_3OH} + 2A_{CH_3OCH_3} \times f_{CH_3OCH_3}}$$
$$\times (1 - S_{CO}) \times 100\%$$

$$STY(CH_3OH) = \frac{GHSV}{\rho \times \omega\% \times 22.4} \times V\%(CO_2)$$
$$\times X(CO_2) \times S(CH_3OH) \times M_{CH_3OH}$$

GHSV (h^{-1}) is the gas hourly space velocity, ρ (kg m^{-3}) is the density of the catalyst and ω (%) represents the mass fraction of Cu.

3. Results and discussion

Fig. 1 shows the transmission electron microscopy (TEM) images of the catalysts prepared by the traditional impregnation method and double solvent method. It shows that the

4370 | *Catal. Sci. Technol.*, 2021, **11**, 4367–4375

This journal is © The Royal Society of Chemistry 2021

impregnation method resulted in a large amount of metal NPs around 11 nm on the surface of the MOF (Fig. 1a), whereas the double solvent method successfully avoided this phenomenon (Fig. 1b and c). The existence of small NPs is also confirmed by high resolution transmission electron microscopy (HRTEM) (Fig. 1c and d). By using the double solvent method, the small particles are distributed in the MOF uniformly with a size range of 1.2–2.0 nm (Fig. 1c). The loaded two species are clearly observed with interplanar fringes of 2.08 Å and 1.63 Å that belong to Cu (111) and ZnO (110), respectively (Fig. 1e and f).

Energy dispersive X-ray spectroscopy (EDXS) in scanning TEM mode (STEM) also indicates the uniform distribution of Cu and Zn throughout the $Cu/ZnO_x@UiO-66$ sample (Fig. 1g). The Cu and Zn distributions overlap with each other, suggesting that Cu and Zn are well-mixed with no obvious phase separation on a length scale of around 10 nm, which has a great effect on the catalytic performance. It is worth noting that the powder X-ray diffraction (PXRD) pattern does not show any characteristic peaks of the metal, which further confirms that the sizes of the nanoparticles are quite small (Fig. 2a). These data indicate that the double solvent method is an effective way to introduce and confine small nanoparticles inside MOF structures. It is believed that the weak interaction energy of hexane with the MOF surface and low interfacial tension in water can be beneficial to the dispersion of the Cu precursor inside the pore network.

The PXRD patterns of UiO-66, Cu@UiO-66 and $Cu/ZnO_x@UiO-66$ are shown in Fig. 2a. The main peaks of Cu@UiO-66 are identical to those of UiO-66, indicating that there is no sample decomposition during the preparation. $Cu/ZnO_x@UiO-66$ shows a slight decrease of crystallinity due

to the Zn precursor reacting with the SBUs of UiO-66. Nitrogen adsorption–desorption experiments show BET surface areas of 262 m^2 g^{-1} for Cu@UiO-66 and 64 m^2 g^{-1} for $Cu/ZnO_x@UiO-66$, which are lower than that of the parent UiO-66 (1112 m^2 g^{-1}). The decreased BET surface areas could be attributed to the decreased crystallinity and potential pore blocking by high metal (both Cu and Zn) loading which is up to 15 wt%. The result of temperature programmed reduction with hydrogen (H_2-TPR) shows an obvious peak at around 250 °C which is the point where Cu^{2+} exposed to air can be reduced (Fig. S3†). The final $Cu/ZnO_x@UiO-66$ was obtained after being reduced under the conditions of 250 °C, 0.1 MPa and 5% H_2–Ar flow from $Cu@UiO-66-(\mu_3-OZnEt)$.

H_2 and CO_2 temperature programmed desorption (TPD) experiments were conducted with the temperature being increased from 100 °C to 250 °C at a speed of 5 °C min^{-1} and then held at 250 °C for 1 h. For H_2-TPD (Fig. 2c), the left two peaks are attributed to the desorption of H_2 left from the Zr-oxide cluster and the third peak is assigned to the H_2 from the ZnO_x sites.[23] The desorption of CO_2 begins at around 135 °C over the pure UiO-66 (Fig. 2d), which is attributed to unsaturated Zr sites on the SBUs of UiO-66. A new peak appears when compared with that of UiO-66 and the desorption temperature decreases to 100 °C after loading Cu into UiO-66, which mainly results from the Cu sites that show relatively low desorption temperature. When Zn species are introduced into the catalyst, the newly appeared peak becomes stronger under the same conditions.[23,31] This result shows that the ZnO_x sites enhance the adsorption capacity of the catalyst for CO_2, which is one of the important factors affecting the catalytic performance.

According to the calculation, the ratio of Zn to Zr should be 2 : 3.[32] However, during the preparation, it was found that the content of Zn is determined partially by the amount of Cu (Fig. 3a). When the amount of Cu is low, some residual Zn could be confined in the MOF's channels and pores. When the loading amount of Cu is high, the content of Zn will be lower than the calculated result due to the steric hindrance effect caused by the preferential entry of Cu into the channel. As a result, the ratio of these three metals can be adjusted by controlling the amount of Cu.

The catalytic performance of $Cu/ZnO_x@UiO-66$ was tested for CO_2 hydrogenation at 180–260 °C and 4.0 MPa with a H_2/CO_2 ratio of 3. The as-prepared $Cu/ZnO_x@UiO-66$ catalysts with different loadings of Cu and Zn are denoted as Cat-X (X refers to the weight percentage of Cu, wt%). The conversion increases with increasing temperature while the selectivity decreases at higher temperature. (Fig. 3b and c) Among these catalysts, Cat-5.86 shows the best catalytic performance with a space–time yield of MeOH (STY_{MeOH}) of 1.27 $kg_{(MeOH)}$ $kg_{(Cu)}^{-1}$ h^{-1} at a gas hourly space velocity (GHSV) of 12 000 h^{-1} (T = 250 °C). Under the same catalytic conditions, the STY_{MeOH} value greatly exceeds those of the commercial Cu/ZnO/Al_2O_3 catalyst (0.23 $kg_{(MeOH)}$ $kg_{(Cu)}^{-1}$ h^{-1}) and Cu/ZnO on UiO-66 (0.15 $kg_{(MeOH)}$ $kg_{(Cu)}^{-1}$ h^{-1}) prepared with the traditional impregnation method (Table 1). This is partially

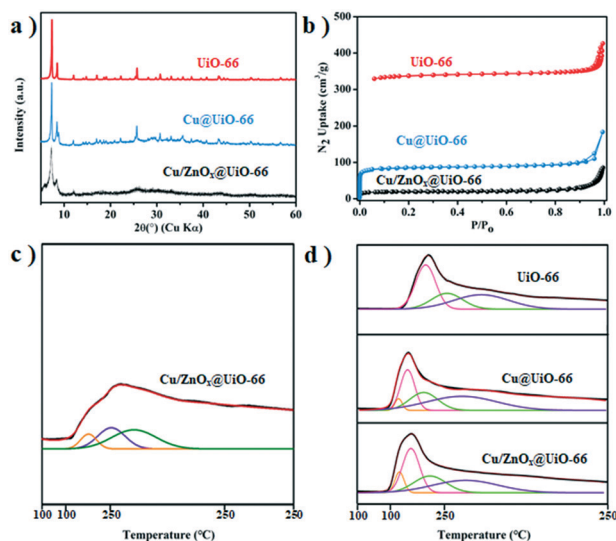

Fig. 2 (a) Powder X-ray diffraction patterns. (b) Nitrogen sorption isotherms (77 K) for UiO-66 (S_{BET} = 1112 m^2 g^{-1}) and its metallated derivatives Cu@UiO-66 (S_{BET} = 262 m^2 g^{-1}) and $Cu/ZnO_x@UiO-66$ (S_{BET} = 64 m^2 g^{-1}). (c) H_2-TPD profile of $Cu/ZnO_x@UiO-66$. (d) CO_2-TPD profiles of UiO-66, Cu@UiO-66 and $Cu/ZnO_x@UiO-66$.

This journal is © The Royal Society of Chemistry 2021
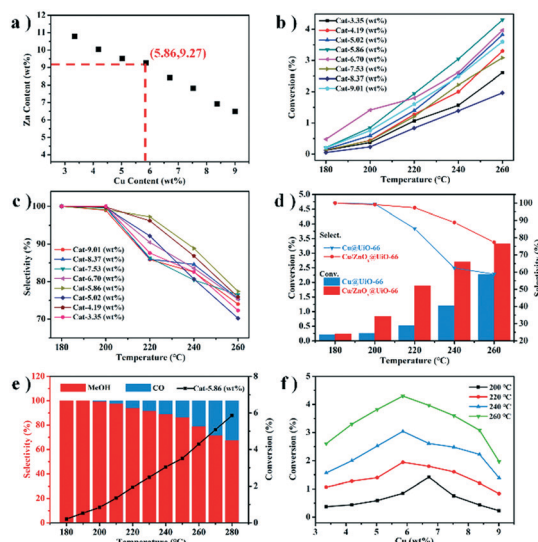
Catal. Sci. Technol., 2021, 11, 4367–4375 | 4371

Fig. 3 (a) The relationship between the contents of Zn and Cu. (b) Conversion rate of catalysts with different Cu/Zn ratios *vs.* temperature. (c) Selectivity of catalysts with different Cu/Zn ratios *vs.* temperature. (d) The catalytic performance of Cu/ZnO$_x$@UiO-66 and Cu@UiO-66 (P = 4.0 MPa, T = 250 °C, GHSV = 12 000 h^{-1}). (e) Selectivity and conversion rate of Cu/ZnO$_x$@UiO-66 (Cu-5.86 wt%) *vs.* GHSV (P = 4.0 MPa, T = 250 °C). (f) Conversion rate of catalysts with different Cu/Zn ratios *vs.* the content of Cu.

sites exposed to the surface of the catalyst account for only 13.9% of the total sites. This result from another side proves the high efficiency of these 13.9% sites. By contrast, a TOF value of only 0.48 × 10^{-3} s^{-1} was obtained for Cu/ZnO on UiO-66 prepared with the traditional impregnation method. It is worth noting that compared with the literature reported catalysts, Cat-5.86 synthesized in this work also shows very competitive and impressive performance (Table S1†).

Although there is no final conclusion on the mechanism of Cu–Zn catalysts,[1] the addition of Zn undoubtedly affects the catalytic performance. Cu@UiO-66 without Zn which was prepared for comparison showed low activity and selectivity (Fig. 3d and Table 1). After loading Zn, the activity was obviously improved and the certain ratio of Cu/Zn was given by ICP-OES. The performance curve showed an obvious volcanic shape after increasing the Cu content gradually and the optimal value was obtained when the mass fraction of Cu reached around 5.86%, giving a selectivity of 78.8% and a conversion rate of 4.3% at a GHSV of 12 000 h^{-1} (260 °C) (Fig. 3f).

Cat-5.86 was tested through a 100 h catalytic process to show its stability performance, which is an important index. It can be seen from the results that the catalyst exhibits good stability only with a slight decrease (~4%) in selectivity (Fig. 4). Generally, the performance of Cu-based catalysts will decrease obviously due to the sintering and phase separation in the long-term catalytic process, but in our work this phenomenon has been alleviated greatly by using the as-prepared Cu/ZnO$_x$@UiO-66.

These results confirm that small Cu/ZnO$_x$ NPs could be obtained *via* the double solvent method, playing a key role in highly efficient hydrogenation of CO$_2$. UiO-66, as a porous supporter, even without organic functional coordinating groups, could confine the growth of the NPs, which also substantially improves the stability of the catalyst. Although its small pore size and large amounts of organic ligands reduced the number of active catalytic sites (13.9%) that could expose to the surface for the catalytic activity, the efficiency of these active sites is satisfactory. At the same time, the Zn loaded in the second step to obtain Cu/ZnO$_x$@UiO-66 not only cooperated with Cu to help improve the catalytic activity, but also reduced the exposure to the Cu surface, thus reducing the generation of CO.

attributed to the fact that even with a low loading of metal, the catalyst synthesized by the double solvent method could catalyze the CO$_2$ hydrogenation quite effectively. In addition, Cat-5.86 shows a great improvement in the methanol selectivity compared with the traditional Cu-based catalyst, giving a value of 86.1%.[33–35] CO, the main by-product, was well suppressed during the catalytic process, which is due to the uniform distribution of metal nanoparticles and the reduced number of single Cu NPs. Generally, a low GHSV value benefits the conversion rate while a high GHSV value has a reverse effect. However, after we lowered the GHSV value to 1500 h^{-1}, its selectivity just decreased a little from 86.1% to 82.4%, and its conversion rate increased from 3.5% to 7.3%. We also calculated the TOF values of methanol formation over different kinds of catalysts. Cat-5.86 gives a very high TOF value of 5.08 × 10^{-3} s^{-1} at a GHSV of 12 000 h^{-1} although the catalytic

Table 1 Catalytic performance comparison of different catalysts

	Cu (wt%)	Gas flow	CO$_2$ conv. (%)	Select. (%)	STY (kg$_{(MeOH)}$ kg$_{(Cu)}^{-1}$ h^{-1})	TOF × 10^3 (s^{-1})
Cu/ZnO$_x$@UiO-66	5.86	18 000 (h^{-1})	3.00	87.5	1.66	6.62
	5.86	12 000 (h^{-1})	3.51	86.1	1.27	5.08
	5.86	6000 (h^{-1})	4.39	84.2	0.78	3.12
	5.86	1500 (h^{-1})	7.33	82.4	0.32	1.28
Cu@UiO-66	6.65	12 000 (h^{-1})	1.72	60.2	0.38	1.53
Cn/ZnO on UiO-66	6.21	12 000 (h^{-1})	0.44	85.3	0.15	0.48
Cu/ZnO/Al$_2$O$_3$	50.13	12 000 (h^{-1})	9.72	47.2	0.23	—
	50.13	6000 (h^{-1})	10.24	40.1	0.10	—

The percentage of Cu on the NP surface (measured by N$_2$O oxidation followed by H$_2$ titration): D_{Cu} (Cu/ZnO$_x$@UiO-66) = 13.9%, D_{Cu} (Cu@UiO-66) = 15.2%, D_{Cu} (Cu/ZnO on UiO-66) = 14.8%; reaction conditions: T = 250 °C, P = 4.0 MPa (H$_2$/CO$_2$ = 3).
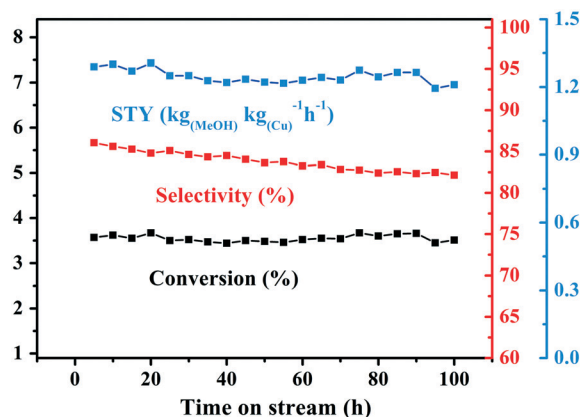

Fig. 4 STY, conversion rate and selectivity *vs.* time over a period of 100 h on stream (T = 250 °C, P = 4.0 MPa, GHSV = 12 000 h^{-1}).

In order to understand the valence states of these three metals in the catalyst during the process, X-ray photoelectron spectroscopy (XPS) and LMM Auger spectroscopy were used to show the changes before and after being treated with reaction gases. Cu exists in the form of Cu(0) after being reduced by NaBH$_4$ and can remain unchanged under the reducing atmosphere of the reaction gases (Cu 2p$_{3/2}$ peak at 932.6 eV and Cu LMM Auger spectral peak at 567.9 eV) (Fig. 5a and b). The XPS characteristic peaks of Zr obviously shift towards low binding energy, which shows the presence of Zr(III) reduced from Zr(IV) (Fig. 5c). The valence change of Zr was caused by the strong reducing substances produced in the process.[23] The existence form of Zn(II) in the catalyst is verified through the above analyses of FT-IR, GC-MS and HRTEM. Furthermore, the XPS result also shows the presence of the Zn(II)(ZnO) peak at 1021.7 eV (Fig. 5d). However, after the treatment of reaction gases, the peak of Zn(0) appears at 496 eV from the Auger spectra (Fig. 5e). Thus, the composition of Cu/ZnO@UiO-66 becomes Cu/ZnO$_x$@UiO-66 during the reaction, for which XPS demonstrates that the Cu^{x+} was reduced into Cu(0) completely while Zn(0) and Zn(II) existed simultaneously in the sample because Zn(II) was partially reduced to Zn(0) by the spillover hydrogen in the reaction. The mixed species of Cu and Zn do help to achieve a better performance (Fig. 3d and Table 1), which is consistent with the conclusion reported in the literature.[23]

In situ DRIFTS was conducted to determine the existing intermediates during the catalytic process over Cu/ZnO$_x$@UiO-66, from which we can have a rough idea about its possible catalytic mechanism (Fig. 5f). The bands at 1049 cm^{-1} and 1150 cm^{-1} are assigned to the ν(CO) modes of bridged and terminal methoxide species, respectively. The two bands at 1367 cm^{-1} and 1581 cm^{-1} are attributed to the antisymmetric and symmetric OCO stretching vibrations of adsorbed bidentate *HCOO species on Cu/ZnO$_x$@UiO-66. The band at 2890 cm^{-1} is assigned to stretching (ν(CH)) vibrations and the band at 2974 cm^{-1} may be attributed to the CH bending and asymmetric OCO stretching modes.[22,23] According to the above analysis, a possible mechanism is proposed. Firstly,
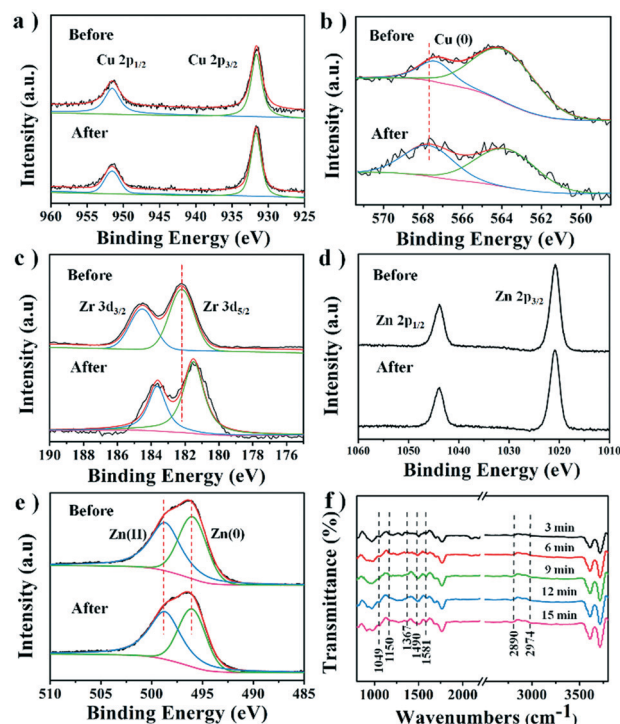

Fig. 5 (a)–(e) XPS spectra of Cu 2p, Cu LMM Auger spectra of Cu/ZnO$_x$@UiO-66 (the peak at 564.5 eV represents another Auger transition level of Cu LMM),[36] XPS spectra of Zr 3d and Zn 2p, and Zn LMM Auger spectra of Cu/ZnO$_x$@UiO-66 (before and after being treated with reaction gases under the reaction conditions). (f) DRIFTS profiles of Cu/ZnO$_x$@UiO-66 and the corresponding peaks of intermediates.

H$_2$ undergoes homolytic dissociation on the Cu surface. Some of the hydrogen connects with Cu to form Cu–H species and the rest of the hydrogen spills to the Zr sites and ZnO$_x$ sites due to the overflow effect where CO$_2$ can be captured and translated into carbonates at the same time. Then the carbonates could be hydrogenated quickly to generate the bidentate *HCOO species owing to the effect of activated and overflowing hydrogen. Finally, methanol is synthesized from combining the *HCOO species and hydrogen. This also proves that Cu/ZnO$_x$@UiO-66 is more like a ternary catalyst and its Zr SBUs also promoted the reaction.[23]

4. Conclusions

In summary, this work demonstrates that the MOF/nanoparticle composites synthesized by the double solvent method show enhanced catalytic properties for CO$_2$ hydrogenation when compared with the commercialized catalyst and catalyst prepared with the traditional impregnation method. This is the first work to realize controllable bimetallic synthesis inside UiO-66 by the double solvent method. The double solvent method solves the problems that metal particles are easy to agglomerate and Cu and ZnO phases are easy to separate during the high temperature reaction process, thus the prepared catalyst could show good stability which is very

important for industrial application. We anticipate that this method could also be used to synthesize a variety of other MOF/nanoparticle composites to enhance their performance in a number of catalytic reactions especially for MOFs without organic coordinating groups.

Author contributions

Yang Yang and Yanan Xu conducted the study. Heng Ding, Dong Yang, Enping Cheng and Yiming Hao implemented some experiments of material synthesis. Hongtao Wang, Yanzhen Hong and Yuzhong Su worked on the characterization studies. Yang Yang, Yanliang Wang and Yanan Xu analysed the data. Li Peng and Jun Li supervised the work. Yanan Xu, Yanliang Wang, Li Peng and Jun Li wrote the manuscript. All the authors participated in discussion of this research work.

Conflicts of interest

There are no conflicts to declare.

Acknowledgements

Notes and references

1 S. Kattel, P. J. Ramirez, J. G. Chen, J. A. Rodriguez and P. Liu, *Science*, 2017, **355**, 1296–1299.

2 J. Wang, G. Li, Z. Li, C. Tang, Z. Feng, H. An, H. Liu, T. Liu and C. Li, *Sci. Adv.*, 2017, **3**, e1701290.

3 R. Gaikwad, H. Reymond, N. Phongprueksathat, P. Rudolf von Rohr and A. Urakawa, *Catal. Sci. Technol.*, 2020, **10**, 2763–2768.

4 X. Dong, F. Li, N. Zhao, F. Xiao, J. Wang and Y. Tan, *Appl. Catal., B*, 2016, **191**, 8–17.

5 J. Sloczynski, R. Grabowski, P. Olszewski, A. Kozlowska, J. Stoch, M. Lachowska and J. Skrzypek, *Appl. Catal., A*, 2006, **310**, 127–137.

6 M. Gentzen, W. Habicht, D. E. Doronkin, J. D. Grunwaldt, J. Sauer and S. Behrens, *Catal. Sci. Technol.*, 2016, **6**, 1054–1063.

7 T. Inui, H. Hara, T. Takeguchi and J. B. Kim, *Catal. Today*, 1997, **36**, 25–32.

8 P. Gao, F. Li, H. Zhan, N. Zhao, F. Xiao, W. Wei, L. Zhong, H. Wang and Y. Sun, *J. Catal.*, 2013, **298**, 51–60.

9 A. Karelovic and P. Ruiz, *Catal. Sci. Technol.*, 2015, **5**, 869–881.

10 X. Dong, H. B. Zhang, G. D. Lin, Y. Z. Yuan and K. R. Tsai, *Catal. Lett.*, 2003, **85**, 237–246.

11 B. A. Peppley, J. C. Amphlett, L. M. Kearns and R. F. Mann, *Appl. Catal., A*, 1999, **179**, 21–29.

12 M. B. Fichtl, D. Schlereth, N. Jacobsen, I. Kasatkin, J. Schumann, M. Behrens, R. Schlögl and O. Hinrichsen, *Appl. Catal., A*, 2015, **502**, 262–270.

13 F. Liao, Y. Huang, J. Ge, W. Zheng, K. Tedsree, P. Collier, X. Hong and S. C. Tsang, *Angew. Chem., Int. Ed.*, 2011, **50**, 2162–2165.

14 T. Lunkenbein, J. Schumann, M. Behrens, R. Schlögl and M. G. Willinger, *Angew. Chem., Int. Ed.*, 2015, **54**, 4544–4548.

15 Y. Bai, Y. B. Dou, L. H. Xie, W. Rutledge, J. R. Li and H. C. Zhou, *Chem. Soc. Rev.*, 2016, **45**, 2327–2367.

16 L. Peng, S. Yang, D. T. Sun, M. Asgari and W. L. Queen, *Chem. Commun.*, 2018, **54**, 10602–10605.

17 H. C. Zhou, J. R. Long and O. M. Yaghi, *Chem. Rev.*, 2012, **112**, 673–674.

18 N. A. Khan, Z. Hasan and S. H. Jhung, *J. Hazard. Mater.*, 2013, **244–245**, 444–456.

19 C.-H. Yu, C.-H. Huang and C.-S. Tan, *Aerosol Air Qual. Res.*, 2012, **12**, 745–769.

20 F. X. L. I. Xamena, O. Casanova, R. G. Tailleur, H. Garcia and A. Corma, *J. Catal.*, 2008, **255**, 220–227.

21 J. Lee, O. K. Farha, J. Roberts, K. A. Scheidt, S. T. Nguyen and J. T. Hupp, *Chem. Soc. Rev.*, 2009, **38**, 1450–1459.

22 B. Rungtaweevoranit, J. Baek, J. R. Araujo, B. S. Archanjo, K. M. Choi, O. M. Yaghi and G. A. Somotjai, *Nano Lett.*, 2016, **16**, 7645–7649.

23 B. An, J. Zhang, K. Cheng, P. Ji, C. Wang and W. Lin, *J. Am. Chem. Soc.*, 2017, **139**, 3834–3840.

24 N. Van, L. Loc, N. Tri and H. Cuong, *Int. J. Nanotechnol.*, 2015, **12**, 405.

25 J. C. Wang, Y. H. Hu, G. J. Chen and Y. B. Dong, *Chem. Commun.*, 2016, **52**, 13116–13119.

26 D. Esken, X. Zhang, O. I. Lebedev, F. Schröder and R. A. Fischer, *J. Mater. Chem.*, 2009, **19**, 1314–1319.

27 M. J. Katz, Z. J. Brown, Y. J. Colon, P. W. Siu, K. A. Scheidt, R. Q. Snurr, J. T. Hupp and O. K. Farha, *Chem. Commun.*, 2013, **49**, 9449–9451.

28 A. Schaate, P. Roy, A. Godt, J. Lippke, F. Waltz, M. Wiebcke and P. Behrens, *Chem*, 2011, **17**, 6643–6651.

29 M. Kandiah, M. H. Nilsen, S. Usseglio, S. Jakobsen, U. Olsbye, M. Tilset, C. Larabi, E. A. Quadrelli, F. Bonino and K. P. Lillerud, *Chem. Mater.*, 2010, **22**, 6632–6640.

30 L. Valenzano, B. Civalleri, S. Chavan, S. Bordiga, M. H. Nilsen, S. Jakobsen, K. P. Lillerud and C. Lamberti, *Chem. Mater.*, 2011, **23**, 1700–1718.

31 M. Mihet, G. Blanita, M. Dan, L. Barbu-Tudoran and M. D. Lazar, *J. Nanosci. Nanotechnol.*, 2019, **19**, 3187–3196.

32 S. Devautour-Vinot, G. Maurin, C. Serre, P. Horcajada, D. Paula da Cunha, V. Guillerm, E. de Souza Costa, F. Taulelle and C. Martineau, *Chem. Mater.*, 2012, **24**, 2168–2177.

33 S. Li, L. Guo and T. Ishihara, *Catal. Today*, 2020, **339**, 352–361.

34 M. Mureddu, F. Ferrara and A. Pettinau, *Appl. Catal., B*, 2019, **258**, 117941.

4374 | *Catal. Sci. Technol.*, 2021, **11**, 4367–4375

This journal is © The Royal Society of Chemistry 2021

35 G. Wang, D. Mao, X. Guo and J. Yu, *Int. J. Hydrogen Energy*, 2019, **44**, 4197–4207.

36 Y. P. Timalsina, M. Washington, G.-C. Wang and T.-M. Lu, *Appl. Surf. Sci.*, 2016, **363**, 209–216.